Sulphur Hexafluoride: Low energy (e,2e) experiments and molecular three-body distorted wave theory

DOI:
10.1088/0953-4075/49/19/195203

Document Version
Accepted author manuscript

Sulphur Hexafluoride: Low energy (e,2e) experiments and molecular three-body distorted wave theory

Kate L Nixon[1,2], Andrew J Murray[1], H Chaluvadi[3], C G Ning[4], James Colgan[5] and Don H Madison[3]

[1]Photon Science Institute, School of Physics & Astronomy, University of Manchester, Manchester M13 9PL, UK

[2]School of Biology, Chemistry and Forensic Science, University of Wolverhampton, Wolverhampton WV1 1LY, UK

[3]Department of Physics, Missouri University of Science and Technology, Rolla MO 65409, USA

[4]Department of Physics, State Key Laboratory of Low-Dimensional Quantum Physics, Tsinghua University, Beijing 100084, China

[5]Theoretical Division, Los Alamos National Laboratory, Los Alamos, NM 87545

Abstract

Experimental and theoretical triple differential ionisation cross-sections (TDCS's) are presented for the highest occupied molecular orbital of sulphur hexafluoride. These measurements were performed in the low energy regime, with outgoing electron energies ranging from 5 to 40 eV in a coplanar geometry, and with energies of 10 and 20 eV in a perpendicular geometry. Complementary theoretical predictions of the TDCS were calculated using the molecular three-body distorted wave formalism. Calculations were performed using a proper average over molecular orientations as well as the orientation-averaged molecular orbital approximation. This more sophisticated model was found to be in closer agreement with the experimental data, however neither model accurately predicts the TDCS over all geometries and energies.

1. Introduction

Sulphur hexafluoride (SF_6) is an important molecule that is used in many technological and industrial applications due to its physical properties of being non-flammable, non-toxic, non-corrosive and relatively inert. Its primary use is as a common insulating gas in the electrical industry, due to SF_6 having an electrical breakdown strength three times that of air. SF_6 is used as a plasma etching gas in

the semiconductor industry, and is also used during the manufacture of magnesium to protect the molten magnesium from oxidants such as air. Additionally, it is used as the halogen donor in rare gas–halide excimer lasers. While SF_6 is an important gas with many applications, the use of this gas is carefully monitored and controlled, as SF_6 is a known greenhouse gas which has a very high global warming potential (GWP). SF_6 has a strong absorption band in the infra-red, and as such effectively traps radiation that normally is emitted from the earth into space. Further, since SF_6 has a low probability of photo-dissociation in the atmosphere, this molecule has a very long lifetime in the stratosphere, which contributes further to its high GWP ranking.

There have been a multitude of experimental investigations of electron collisions with SF_6. Initially, these processes were studied due to SF_6 having a series of shape resonances [1]. Experiments detailing electron-SF_6 collisions continued as the industrial applications of this molecule became evident, and so accurate cross sections were necessary to understand these interactions. The most recent review of Chrisophorou and Olthoff [2] gives a comprehensive summary of previous work from this target. Despite a large number of experimental and theoretical investigations, there has only been one other differential ionisation study that was conducted by Stefani and co-workers [3]. This (e,2e) study was conducted in the high energy electron momentum spectroscopy energy regime [4], where the electronic structure of the molecular orbitals is measured. In the current investigation the (e,2e) technique is used at low incident energies, so as to probe the more complex collision mechanisms for electron impact ionisation of this target.

The (e,2e) technique measures a triple differential cross section (TDCS), and so the data are kinematically complete. The measurements therefore provide the most sensitive test of theoretical models that are developed to describe these ionising collisions. However, for electron impact ionization of molecules, the present experiments cannot resolve the orientation of the target. It is therefore necessary for any theoretical comparison to *incoherently* average the calculated TDCS over all possible orientations of the molecule. Theoretical results using the molecular three–body distorted wave (M3DW) approximation with a ‘proper average’ (PA) over molecular orientations [5] are presented, as well as results calculated using the ‘orientation averaged molecular orbital’ (OAMO) approximation.

SF_6 is a highly symmetric molecule, consisting of a single sulphur atom surrounded by six fluorine atoms equally spaced in an octahedral geometry. With the high degree of symmetry inherent in this molecule, it is anticipated that the ‘proper average’ technique should converge more quickly, as fewer discrete orientations are then necessary to approximate the ensemble of randomly orientated molecules in the experiment. Despite this high degree of symmetry, calculation of the electron impact ionization of SF_6 is still difficult. SF_6 contains a large number of electrons (70) that are distributed throughout the molecule, with the inner-core electrons closely bound to the individual sulphur and fluorine atoms.

This target therefore contrasts with previous experimental studies in Manchester [6-9], which utilized targets that have a heavy central atom bonded to light hydrogen atoms (*i.e.* CH_4, NH_3 and H_2O). It was suggested by Toth and Nagy [10] that for CH_4, the observed discrepancy between theory and experiment may be due to the effective nuclear charge distribution being underestimated within the OAMO model. This effective charge arises in the model due to the spherical averaging process, which replaces the nuclear charges with thin spherical surfaces of positive charge whose radii are set to be equal to the distance from the centre of mass to the individual atomic nuclei. As an example, in CH_4 the +4e charge from the hydrogen nuclei is modelled as a thin sphere with a radius equal to the carbon-hydrogen bond length. This positively charged spherical surface effectively reduces the interaction between the incident and outgoing electrons with the individual nuclei, and therefore is predicted to reduce scattering into the backward direction. However, further measurements of this scattering process found this was not the case [11]. Since SF_6 has a nuclear charge of +54e due to the six fluorine atoms that are equi-distant from the centre of mass, it might be expected that the effect of the spherical charge ring due to the fluorine nuclear charge will be exacerbated for this target.

The structure of this paper is as follows. Following this introduction, the salient features of the (e,2e) spectrometer used to measure the TDCS are described in section 2. Section 3 then details the models used to generate the predicted cross sections. Results from experiment and theory are compared in section 4. Data from a coplanar geometry are presented in section 4A, and results from the perpendicular plane geometry are given in section 4B. Conclusions from this work, together with considerations for future studies are outlined in section 5.

2. The Experimental Apparatus

The experimental data presented here were obtained using the computer controlled and computer optimised (e,2e) spectrometer at the University of Manchester. This spectrometer is described elsewhere [12], however for completeness the pertinent details are given here. The spectrometer can operate over a range of geometries from a coplanar geometry, where the momentum of the incident electron $\mathbf{k_0}$ lies in the detection plane defined by the two outgoing electrons $\mathbf{k_1}$, $\mathbf{k_2}$ ($\psi = 0°$), to the perpendicular geometry where $\mathbf{k_0}$ is orthogonal to the detection plane ($\psi = 90°$) (see figure 1). For all geometries from coplanar to the perpendicular plane, a common normalisation point exists for $\xi_1 = \xi_2 = 90°$. The incident electron beam is produced by a two-stage electron gun that has an energy resolution ~ 0.6 eV. The outgoing electron analyzers are mounted on individual turntables that enable them to rotate independently around the detection plane. The experiments in a coplanar geometry detailed here adopt doubly-symmetric kinematics, with $E_1 = E_2 = E$ and $\xi_1 = \xi_2 = \xi$. The TDCS was then obtained by measuring the ionization probability for a range of scattering angles, ξ, at a given energy, E. Data in the perpendicular plane are presented in terms of the mutual angle $\phi = \xi_1 + \xi_2$, since this is the only angle of relevance in this geometry. Equal energies are still employed in the perpendicular geometry, so that once again $E_1 = E_2 = E$.

High purity SF_6 gas (BOC 99.9% [13]) was admitted into the interaction region via a gas jet. The flow of SF_6 was regulated by a needle valve so that the vacuum in the chamber was raised from a base pressure of ~ 6×10^{-7} torr to a stable working pressure of ~ 1.5 x 10^{-5} torr. A low incident electron beam current of ~ 50 nA – 200 nA was adopted for these measurements, due to the small differential cross-sections from SF_6 that were found. While these low incident beam currents resulted in longer accumulation times (typically 1-2 weeks for each set of data), they were necessary to attain a good signal to background ratio. In addition to using low incident beam currents, the pass energy of each electron analyser was also reduced from that normally used for atomic targets, to increase the energy resolution of the spectrometer. This further reduced the coincidence signal, however this was necessary to resolve the two outermost orbitals of SF_6 that are separated by ~1.4 eV (15.7 and 17.0 eV respectively) [14]. The energy resolution for the measurements was determined to be ~0.9 eV from the coincidence binding energy spectrum, as shown in figure 2. Here it can be seen that the highest occupied molecular orbital (HOMO) is well resolved from the next highest occupied molecular orbitals (NHOMO, NHOMO-1), allowing coincidence data to be obtained only from the HOMO.

To ensure the spectrometer remained optimised over the many weeks of data collection, the electrostatic lenses in the apparatus were adjusted under computer control as the experiment progressed, so as to maximise the electron count rate in each analyser. This corrected for any variation in the signals as the analysers rotated back and forth around the detection plane (up to ten sweeps of the detection plane were used to produce the TDCS signals for a given energy, with data being

accumulated at each angle for up to 5000 seconds). The energy of the spectrometer was re-calibrated at the commencement of each new run, by measuring a new coincidence binding energy spectrum and then setting the incident electron energy to the HOMO peak.

The data presented here for a coplanar geometry have been normalised to unity for the largest measurement in the cross sections, since absolute measurements of the TDCS were not obtained. The uncertainty in the measurements at each angle ξ was obtained from the standard error, generated from averaging the data at a given angle for all sweeps of the detection plane. The angular uncertainties in the measurements have contributions from the pencil angle of the incident electron beam and the acceptance angle of the analyzers. This was estimated to be ~ ± 3° for ξ and ~ ± 5° for ϕ.

While the measurements were not absolute, it is possible to inter-normalise the data for coplanar and perpendicular geometries at a given energy since all measurements with $\xi_1 = \xi_2 = 90°$ are independent of the electron gun angle ψ, as noted above. This allows a further comparison to be made between theory and experiment. In the data presented here, this inter-normalisation was possible for outgoing energies of 10 eV and 20 eV, since data was accumulated in both coplanar and perpendicular plane geometries at these energies.

3. Theoretical

The M3DW approximation has been presented elsewhere [15-17] so only a brief outline of the theory will be presented. The TDCS for the M3DW is given by:

$$\frac{d^5\sigma}{d\Omega_a d\Omega_b dE_b} = \frac{1}{(2\pi)^5}\frac{k_a k_b}{k_i}\left(\left|T_{dir}\right|^2 + \left|T_{exc}\right|^2 + \left|T_{dir} - T_{exc}\right|^2\right) \quad (1)$$

where $\vec{k}_i$, $\vec{k}_a$, and $\vec{k}_b$ are the wave vectors for the initial, scattered and ejected electrons, T_{dir} is the direct scattering amplitude, and T_{exc} is the exchange amplitude. The direct scattering amplitude is given by:

$$T_{dir} = \left\langle \chi_a^-(\mathbf{k}_a, \mathbf{r}_1)\chi_b^-(\mathbf{k}_b, \mathbf{r}_2)\mathrm{C}_{ab}(\mathbf{r}_{12})\middle| W \middle|\phi_{Dy}(\mathbf{r}_2, \mathbf{R})\ \ \chi_i^+(\mathbf{k}_i, \mathbf{r}_1)\right\rangle \quad (2)$$

Where r_1 and r_2 are the coordinates of the incident and the bound electrons, $\chi_i^+(\mathbf{k}_i, \mathbf{r}_1)$, $\chi_a^-(\mathbf{k}_a, \mathbf{r}_1)$, and $\chi_b^-(\mathbf{k}_b, \mathbf{r}_2)$ are the distorted waves for the incident, scattered, and ejected electrons respectively, $\phi_{Dy}(\mathbf{r}_2, \mathbf{R})$ is the initial bound-state Dyson molecular orbital, and **R** is the orientation of the molecule.

In the OAMO approximation, we use $\phi_{Dy}^{OA}(\mathbf{r}_2)$ which is the molecular orbital averaged over all orientations **R** instead of $\phi_{Dy}(\mathbf{r}_2,\mathbf{R})$. In the PA calculations, we find the TDCS for each orientation and then we average over all orientations. In M3DW-OAMO calculations, we average all orientations for the molecular orbital once, independent of the kinematics of the collision, and then we find TDCS with a single calculation of the T-matrix which is orders of magnitude faster than the PA calculations. We have shown that the OAMO approximation is good for H_2 [18] but it seems unlikely that this should be a good approximation for more complex molecules. However we think that it is still of interest to see how good or bad it is since it is very difficult (for us) to get access to enough computer time to perform the proper averages so it would be useful to know if there are cases where it can be used. So far, we have found that it is not good for some intermediate sized molecules [6], [18-20], but suprisingly a reasonably good approximation for the big molecules we have examined [21-25]. Evidently, non-spherical effects become less important as the molecular size and complexity increases which seems reasonable.

The molecular wave functions were calculated using density functional theory (DFT) along with the standard hybrid B3LYP [26] functional by means of the ADF 2007 (Amsterdam Density Functional) program [27] with the TZ2P (triple-zeta with two polarization functions) Slater type basis sets.

The factor $C_{ab}(\mathbf{r}_{12})$ is the exact final state Coulomb interaction between the two outgoing electrons which is called the Post Collision Interaction (PCI) [28]. We also used the Ward-Macek (WM) average Coulomb-distortion factor between the two final state electrons [29] and we will compare results obtained using the WM approximation and the exact Coulomb interaction.

In the T-matrix, the perturbation $W = V_i - U_i$ where V_i is the initial state interaction between the projectile and neutral target, and U_i is a spherically symmetric approximation for V_i which is used to calculate the initial-state distorted wave for the incident electron $\chi_i^+(\mathbf{k}_i,\mathbf{r}_1)$.

Details about the calculation of initial and final state distorted waves can be found in Madison and Al-Hagan [28]. For the exchange amplitude, particles 1 and 2 are interchanged in the final state wavefunction in eq. (2).

4. Results and Discussion

4.1 Coplanar Geometry

The experimental data and theoretical predictions for the HOMO of SF_6 are shown in figure 3. Data for five energies are shown, with outgoing electron energies ranging from 40 eV to 5 eV. The data at each angle have relatively large uncertainties, due to the small cross sections that were obtained.

When using doubly symmetric kinematics, the cross section can be considered in two regions; a *forward scattering* region where both outgoing electrons are detected at angles less than $\xi = 90°$, and a *backward scattering* region where the electrons are detected at angles greater than $\xi = 90°$. Under the present kinematic conditions, the cross section must be zero at $\xi = 0°$ and $\xi = 180°$ due to post-collisional interactions. It can be seen from figure 3 that, for the three highest energies utilised here, 40 eV, 30 eV and 20 eV, the data has a dominant structure in the forward scattering region, with a local minimum at $\xi \sim 90°$ and an increase in the cross section in the backward region. The position and magnitude of the backward scattering peak is outside the angular range that is accessible in this spectrometer. When compared to the other molecular targets investigated by this group [6-9], the forward to backward scattering ratio is found to be significantly smaller in SF_6, that is, there is more intensity in the backward direction than has been measured for other targets. This higher ratio may be due to the larger nuclear charge in this molecule. For a given energy, the incident electron therefore appears to experience a greater interaction with the nuclei for this target, which increases the probability of backwards scattering. For E = 40 eV and 30 eV the forward scattering peak exhibits a clear shoulder at $\xi \sim 50°$. A double peak structure of this kind is often attributed to a p-like nature of the target orbital [30, 31]. Figure 4 shows a plot of the HOMO orbital for SF_6 and it is seen that this orbital looks like six isolated p-type orbitals centered on the fluorine nuclei which explains the p-type character of the experimental data. The two PA calculations for 40 and 30 eV also exhibit a small angle double peak structure similar to the data except that the peaks are shifted to larger angles which suggests that PCI is too strong in the theory. In a recent theoretical study by Dorn and co-workers [11], it was shown that the relative ratio of the main peak and shoulder could be altered by varying the contribution from nuclear scattering so it appears that these features are probably a complicated combination of both PCI and nuclear scattering. The origin of these features in the cross section therefore requires further investigation.

As the incident electron energy is lowered the collision occurs over a longer time period, and so the incident and outgoing electron interactions with the nuclear structure of the molecule will increase. It is then expected that a greater relative intensity will be observed in the backward scattering region as the energy reduces. Post-collisional interactions (PCI) will also become more important as the energy is lowered, leading to an increase in the mutual angle between the outgoing electrons. This is manifested in the experimental data by the forward and backward peaks shifting towards $\xi = 90°$. For E = 10 eV, peaks are observed in the experimental data at $\xi \sim 55°$ and 100°. By contrast, a single peak is observed at $\xi \sim 90°$ for E = 5 eV, indicating that the electrons have the highest probability of emerging from the collision back-to-back. Again, these changes are observed in SF_6 at higher

energies than has been seen from the smaller molecular targets that were studied at similar energies [6-9].

In figure 3 the experimental data are compared with theoretical calculations M3DW calculations using the proper average (PA) method and the orientation averaged molecular orbital (OAMO) approximation. There are three theoretical lines in the figure: One for each of the OAMO and PA models where the exact Coulomb interaction has been used for the post-collisional interaction (PCI), and a second prediction from the PA model where PCI has been modelled using the Ward-Macek approximation [28]. The two results from the PA model give largely similar results.

The agreement between experiment and theory for the PA calculation is not as good as was found for 54.4 eV ionization of CH_4 with asymmetric energies and angles where the PA calculation provided a much improved agreement with experiment [5] relative to the OAMO. On the other hand, the two PA calculations are in better overall agreement with experiment that the OAMO results. As noted above, for the two higher energies, there is a qualitative agreement for p-state forward scattering and the exact PCI predicts the shape of the data a little better. On the other hand, the PA method predicts that the TDCS should have more structure than the OAMO method, and also predicts significantly more structure than observed in the experiment. Both methods predict that at high energies the cross section should be dominant in the forward scattering region, and that the relative intensity in the backward direction should increase with decreasing energy, as noted in the above discussion. At the lowest energy, only the PA calculations predict a peak at $\xi \sim 90°$, as is observed in experiment. In the OAMO model a peak occurs at the much higher angle $\xi \sim 120°$, and this model predicts a minimum around $\xi = 90°$. This suggests that the pre-scattering spherical averaging process in the OAMO model is not accessing the essential physics of the interaction in this kinematic region. The evolution of the TDCS calculated in the PA model as the energy is lowered suggests that the peak at $\xi \sim 90°$ is not due to a simple migration of forward and backward peaks towards $\xi = 90°$, but is due to an additional process from the interaction. This is seen at energies of E = 20 eV and below where three peaks are clearly evident as the forward scattering peak, the backward scattering peak, and as a peak at $\xi \sim 90°$.

At higher energies, the OAMO and PA models predict similar peak positions in the forward scattering direction. However, both overestimate the position of the peak relative to the experimental data, giving positions that more closely correspond to the start of the shoulder seen in the data.

Overall the PA model gives significantly better agreement with the coplanar experimental data than the OAMO model, although the PA model predicts a number of structures that were not observed in the data. The closest agreement is seen at E=30 eV and E=20 eV. At the highest energy with E=40 eV, both models predict significantly less backward scattering than observed. Toth and Nagy [32] showed that the theoretical recoil peak could be enhanced by bringing the nuclei closer together and they

attributed this to the model underestimating nuclear scattering. This suggests that the present underestimation of the recoil peak may result from an underestimation of nuclear scattering. The PA model predicts a new feature around $\xi \sim 90°$ at low incident energies which agrees well with the experimental data, although away from this region the model underestimates the relative cross section. Both methods of including PCI give similar results, and therefore it is difficult to judge which is in closer agreement with the experimental data.

4.2 Perpendicular Geometry

Experimental measurements and the theoretical predictions for the TDCS in the perpendicular geometry are shown in figure 5. The figures show two sets of data from the HOMO of SF_6, for outgoing electron energies of 20 eV and 10 eV. In this figure the data is compared with the PA and OAMO theoretical predictions using the exact calculation of the Coulomb interaction for PCI, and also the PA model using the Ward-Macek approximation. The magnitude of the data has been determined by noting that the cross section for $\xi_1 = \xi_2 = 90°$ is independent of the angle ψ of the electron gun so the perpendicular plane results were normalized to the scattering plane results. This allows a comparison of the magnitude of the predicted cross sections, in addition to their shape.

Under these kinematic conditions the measured cross section is found to be relatively flat and featureless over a wide angular range for both energies. In this geometry the cross section must be symmetric around $\phi = 180°$, as is shown in the calculations. This symmetry is well reproduced in the higher energy data. For outgoing electron energies of 10 eV the data have a slight asymmetry around $\phi = 180°$, which indicates either that the uncertainties in the data are under-represented, or that the electron gun angle was not quite at $\psi = 90°$ during the measurements.

For the highest energy with E = 20 eV the broad, flat cross section is seen to decrease in magnitude when $\phi < 80°$, as well as when $\phi > 280°$. Again in this geometry the TDCS must be zero when $\phi = 0°$ and 360° due to post collisional interactions. By contrast, the data for E = 10 eV has a narrower distribution around $\phi = 180°$, although it is difficult to accurately establish at which angles the cross section decreases. There is some evidence that the cross section may be composed of two small peaks either side of $\phi = 180°$ (as seen at E = 20 eV in the PA approximation), however the data does not have sufficient accuracy to definitively establish this.

The theoretical models predict quite different results in this geometry, once again highlighting the sensitivity of the collision to the nuclear structure of the target. The OAMO model predicts a significantly smaller cross section at both energies. At E = 20 eV the OAMO model predicts a minimum at $\phi = 180°$, while the PA model predicts a maximum. In both cases, the models predict

additional structures that are not observed in the data. It is, however, clear that the PA model gives significantly better agreement to experiment at this energy, with the model using exact exchange giving a closer prediction of the magnitude of the cross section relative to that determined experimentally.

For E = 10 eV both models predict a maximum at $\phi = 180°$, however the OAMO model predicts two deep minima that reach zero at $\phi \sim 150°$ and $\phi \sim 210°$. Again, the OAMO dramatically underestimates the magnitude of the cross section. Despite this, the OAMO model more accurately predicts the width of the observed cross section, with the PA model predicting a TDCS that is narrower. However, this is probably fortuitous since the PA calculation should be the more accurate. In figure 5 it can be seen that the PA calculation using the exact form of the post-collisional interaction predicts a slight increase in the wings of the cross section than using the Ward-Macek approximation, which yields a slightly better match to experiment. However, both theories predict a lower intensity than is observed experimentally.

5. Conclusions

Experimental TDCS data and theoretical predictions have been presented for the highly symmetric molecule SF_6. The results show that this molecule produces an increase in backward scattering compared to that observed for smaller molecules. The development and implementation of the 'proper average' description of the interaction as presented here has been a major advancement in improving the of the M3DW model for calculating electron impact ionisation of these complex targets. This model eliminates the need to adopt an orientation averaged orbital prior to the collision which was introduced to make the calculations tractable in terms of computer time. To calculate PA cross sections requires using several thousand processors on a large computer cluster. Implementation of this approach has clearly led to improvements in the comparison of experiment and theory, as demonstrated here. However, the model does not yet accurately predict the present data under a wide range of kinematic conditions. While this theory predicts many of the trends seen in the experiment, the calculation predicts more features than are observed, and does not accurately emulate the cross section in all cases. Other sources of these differences clearly need to be investigated, so as to improve the model in the future. The OAMO approximation was in poor agreement with the present data so it is becoming apparent that this approximation is not going to be useful for intermediate sized molecules. However, it appears to be a reasonably good approximation for the big biomolecules which is very fortunate since, for some of the big molecules, PA calculations are not feasible with present computing resources.

Acknowledgements

KLN would like to thank the European commission for a Marie Curie International Incoming Fellowship at the University of Manchester. We would like to thank the technicians in the Schuster laboratory for providing excellent support for the experimental apparatus. This work was partly supported by the US National Science Foundation under Grant. No. PHY-1068237 and by the National Natural Science Foundation of China under Grants No. 11174175. Computational work was performed with Institutional Computing resources made available through the Los Alamos National Laboratory and XSEDE resources provided by the Texas Advanced Computing Center (Grant No. TG-MCA07S029). The Los Alamos National Laboratory is operated by Los Alamos National Security, LLC, for the National Nuclear Security Administration of the US Department of Energy under Contract No. DE-AC5206NA25396.

References

1. BM Addison-Jone, KH Tan, BW Yates, JN Cutler and GM Bancroft *J. Electron Spectrosc. Relat. Phenom.* **48** 155 (1989)
2. LG Christophorou & JK Olthoff, *J Phys Chem Ref Data* **29** 267 (2000)
3. A Giardini-Guidoni, R Fantoni, R Tiribelli, D Vinciguerra, R Camilloni and G Stefani *J Chem Phys* **71** 3182 (1979)
4. E. Weigold and I. E. McCarthy, *Electron Momentum Spectroscopy* (Kluwer/Plenum, New York, 1999).
5. H Chaluvadi, C Ning and DH Madison *Phys Rev A* **89** 062712 (2014)
6. KL Nixon, AJ Murray, H Chaluvadi, C Ning, J Colgan, and DH Madison *J. Chem. Phys*. **138**, 174304 (2013)
7. KL Nixon, AJ Murray, H Chaluvadi, C Ning and DH Madison, *J Chem Phys* **134** 174304 (2011)
8. KL Nixon, AJ Murray, H Chaluvadi, S Amami, DH Madison and C Ning *J Chem Phys* **136** 094302 (2012)
9. KL Nixon, AJ Murray &C Kaiser, *J. Phys. B* 43 085202 (2010)
10. I Toth and L Nagy, *J Phys B* **43** 135204 (2010)
11. A Senftleben, T Pfluger, X Ren, B Najjari, A Dorn and J Ullrich, *J Phys B* **45** 021001 (2012)
12. A J Murray, B C H Turton and F H Read *Rev. Sci. Inst.* **63** 33465 (1992)
13. BOC Industrial Gases UK: http://www.boconline.co.uk
14. G. Bieri, L. Åsbrink, W. von Niessen *Journal of Electron Spectroscopy and Related Phenomena*, **27** 129 (1982)
15. J Gao, DH Madison and JL Peacher *J. Chem. Phys.* **123** 204314 (2005)
16. J Gao, DH Madison and JL Peacher *Phys. Rev. A* **72** 032721 (2005)
17. J Gao, DH Madison and JL Peacher *J. Chem. Phys.* **123** 204302 (2005)
18. S. Xu, Hari Chaluvadi, X. Ren, T. Pflüger, A. Senftleben, C. G. Ning, S. Yan, P. Zhang, J. Yang, X. Ma, J. Ullrich, D. H. Madison, and A. Dorn, J. Chem. Phys. **137**, 024301 (2012).
19. H. Chaluvadi, C. G. Ning and D. Madison, Phys. Rev. A **89**, 062712 (2014).
20. E. Ali, K. Nixon, A. Murray, C. Ning, J. Colgan, and D. Madison, Phys. Rev. A **92**, 042711 (2015).

21. D. Jones, J. D. Builth-Williams, S. M. Bellm, L. Chiari, H. Chaluvadi, D. Madison, C. Ning, B. Lohmann, O. Ingólfsson, and M. Brunger, Chem. Phys. Let. **572**, 32 (2013).
22. J. D. Builth-Williams, S. M. Bellm, L. Chiari, P. A. Thorn, D. B. Jones, H. Chaluvadi, D. H. Madison, C. G. Ning, B. Lohmann, G. da Silva, and M. J. Brunger, J. Chem. Phys. **139**, 034306 (2013).
23. J. D. Builth-Williams, G. B. da Silva, L. Chiari, D. B. Jones, H. Chaluvadi, D. H. Madison, and M. J. Brunger, J. Chem. Phys. **140**, 214312 (2014).
24. G. B. da Silva, R. F. C. Neves, L. Chiari, D. B. Jones, E. Ali, D. H. Madison, C. G. Ning, K. L. Nixon, M. C. A. Lopes, and M. J. Brunger, J. Chem. Phys. 141, 124307 (2014).
25. D. B. Jones, E. Ali, K. L. Nixon, P. Limão-Vieira, M.-J. Hubin-Franskin, J. Delwiche, C. G. Ning, J. Colgan, A. J. Murray, D. H. Madison, and M. J. Brunger, J. Chem. Phys. **143**, 184310 (2015).
26. C Lee, W Yang, and RG Parr *Phys. Rev. B* **37** 785 (1988)
27. CF Guerra et al. *Theor. Chem. Acc.* **99** 391 (1998)
28. DH Madison and O Al-Hagan, *Journal of Atomic, Molecular, and Optical Physics* **2010** 367180 (2010).
29. SJ Ward and JH Macek, *Phys. Rev. A* **49** 1049 (1994)
30. AJ Murray, MJ Bowring and FH Read J. Phys. B **33** 28598 (2000)
31. MA Stevenson, LR Hargreaves, B Lohmann, I Bray, D Fursa, K Bartschat and A Kheifets, Phys. Rev. A **79** 012709 (2009)
32. I Toth and L Nagy J. Phys. B. **44** 195205 (2011)

Figure 1: Schematic of the experimental geometries used in this study. A coplanar geometry ($\psi = 0°$) is defined when the incident electron momentum $\mathbf{k_0}$ lies in the detection plane defined by $\mathbf{k_1}$ and $\mathbf{k_2}$. The analyzer angles (ξ_1 and ξ_2) are measured with respect to the projection of the incident electron momentum $\mathbf{k_0}$ in this plane, as shown. The perpendicular geometry is accessed by moving the electron gun to an angle $\psi = 90°$. In this geometry the only relevant angle is the mutual angle $\phi = \xi_1 + \xi_2$ between the two analyzers.

Figure 2: A typical coincidence binding energy spectrum obtained for SF_6. The experimental data is shown, and the dotted curve is a fit of two Gaussians to the data. This spectrum was measured in a coplanar geometry with outgoing electron energies E = 20 eV at an angle $\xi = 45°$. The peak at lower energies (15.7 eV) is due to the HOMO, that at the higher energy (17.2 eV) is attributed to the NHOMO and NHOMO-1 orbitals that are almost degenerate. The data demonstrate that good separation has been achieved using the current experimental energy resolution, so that the TDCS data can be attributed to the HOMO only.

Figure 3: TDCS from the HOMO of sulphur hexafluoride for coplanar symmetric kinematics. Incident energies (E_0) of 10 – 80 eV above the ionisation potential (15.7 eV) where used. The energies of the outgoing electrons (E_1 and E_2) satisfy the conservation of energy such that $E_0 + IP = E_1 + E_2$. The energies shown on the respective plots are those of the outgoing electron where $E_1 = E_2 = E$, as defined by the doubly symmetric geometry employed. The energies of the outgoing electrons are shown in the respective plots where $E_1 = E_2 = E$. The experimental data (dots) and results from the molecular three-body distorted wave approximation (lines) are shown. Calculations using the proper average (PA) over molecular orientations and the post collision interaction (PCI) treated exactly (Ex) are shown in the solid red curve, while the green dotted curve shows results in which the Ward-Macek approximation (WM) has been used to represent PCI. The calculation using the orientation averaged molecular orbital (OAMO) approximation and exact PCI is the blue dashed curve. The experimental and theoretical data have been independently normalized to unity at the highest intensity for each energy.

Figure 4. Plot of SF_6 HOMO wavefunction. The individual p-type orbitals are all centered on the fluorine nuclei.

Figure 5: Experimental and theoretical TDCS for the HOMO of SF_6 for the perpendicular geometry. Incident energies of 40 and 20eV above the ionisation potential were used, corresponding to outgoing energies of 20 and 10eV respectively, as indicated on the respectively plots. Three theoretical predictions are shown for all energies. Calculations using the proper average (PA) over molecular orientations and the post collision interaction (PCI) treated exactly (Ex) are shown in the solid red curve, while the green dotted curve shows results in which the Ward-Macek approximation (WM) has been used to represent PCI. The calculation using the orientation averaged molecular orbital (OAMO) approximation and exact PCI is the blue dashed curve. The experimental and theoretical data have been normalized to the coplanar data at $\xi_1 = \xi_2 = 90°$, or $\phi = 180°$, as discussed in the text. The TDCS must be symmetric around $\phi = 180°$, and so the small variations in the data for E = 10eV are attributed to the low coincidence yields that were obtained at this energy.

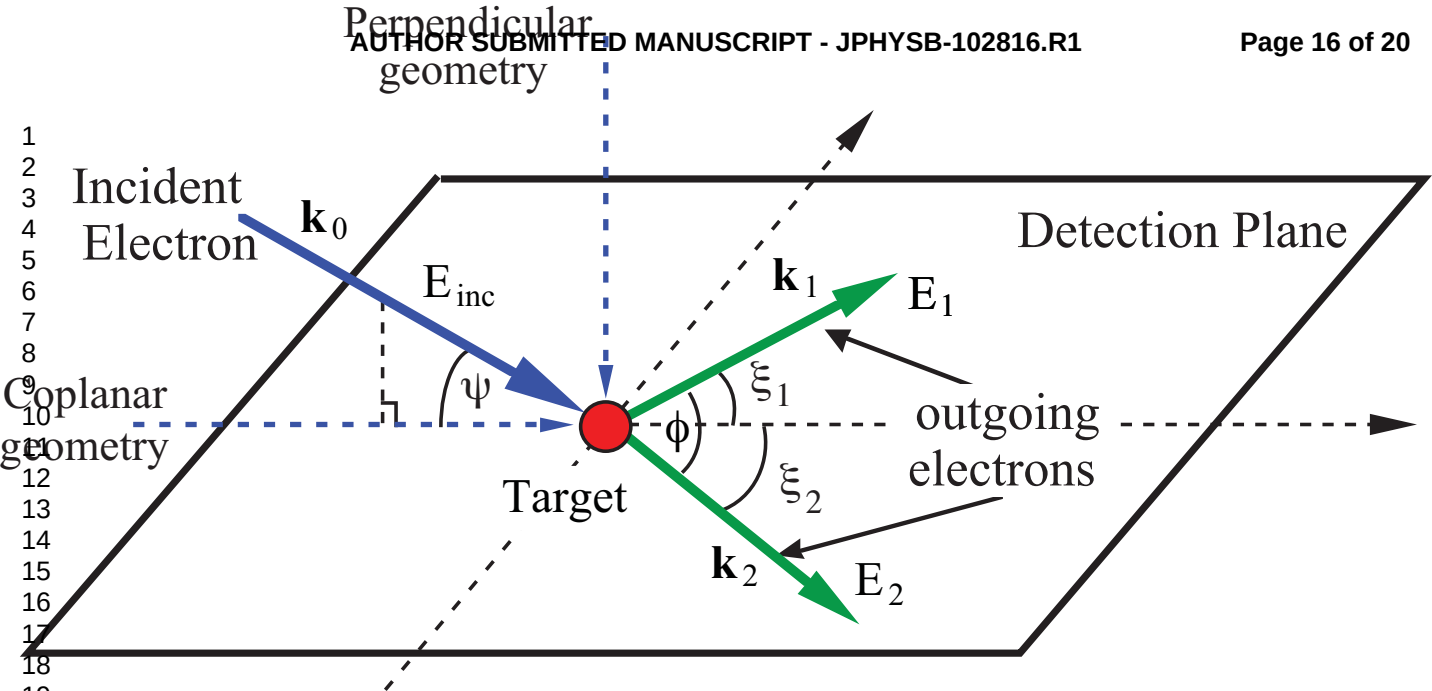
Perpendicular geometry
Incident Electron
$\mathbf{k}_0$
E_{inc}
Detection Plane
$\mathbf{k}_1$
E_1
ψ
ξ_1
Coplanar geometry
ϕ
outgoing electrons
Target
ξ_2
$\mathbf{k}_2$
E_2

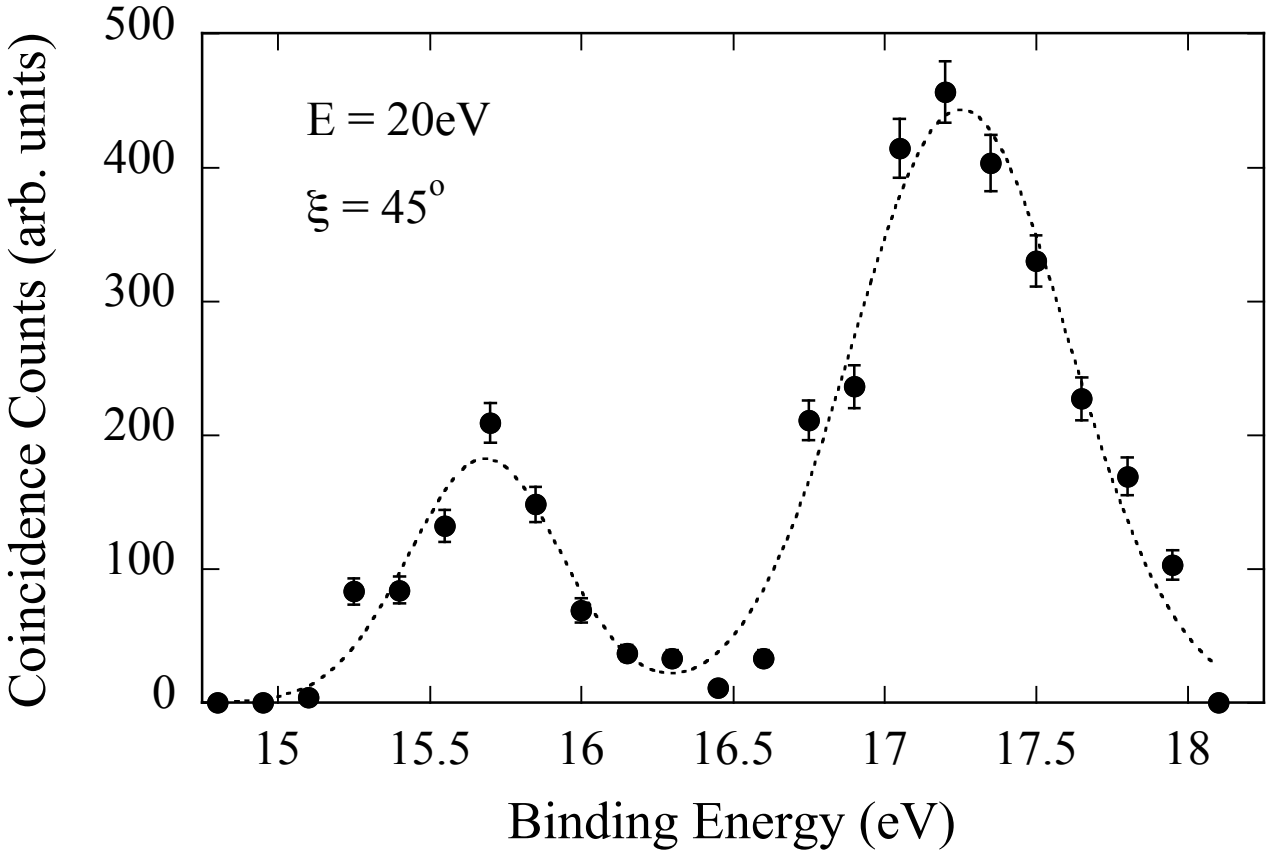
E = 20eV
ξ = 45°
Coincidence Counts (arb. units)
Binding Energy (eV)
0
100
200
300
400
500
15
15.5
16
16.5
17
17.5
18

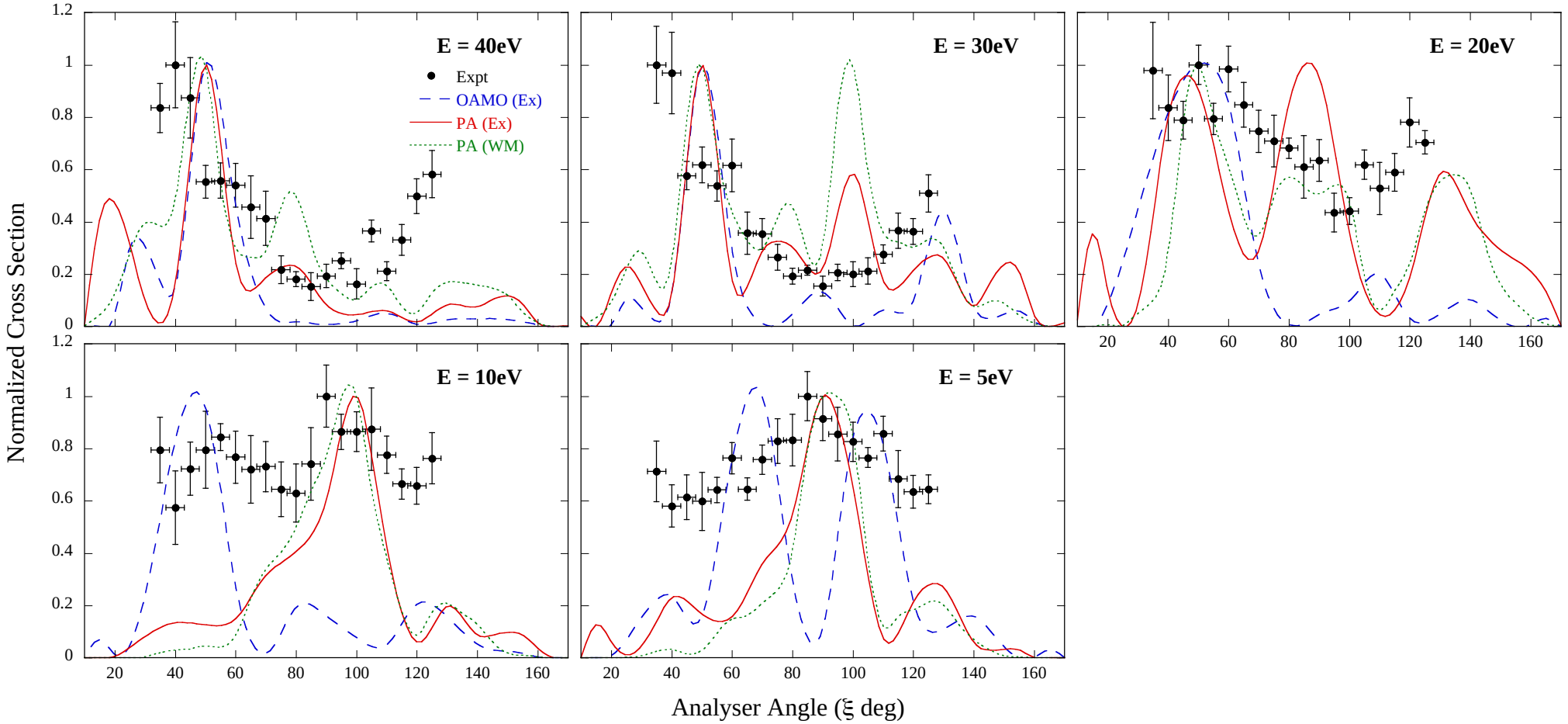
E = 40eV
Expt
OAMO (Ex)
PA (Ex)
PA (WM)
E = 30eV
E = 20eV
E = 10eV
E = 5eV
Normalized Cross Section
Analyser Angle (ξ deg)

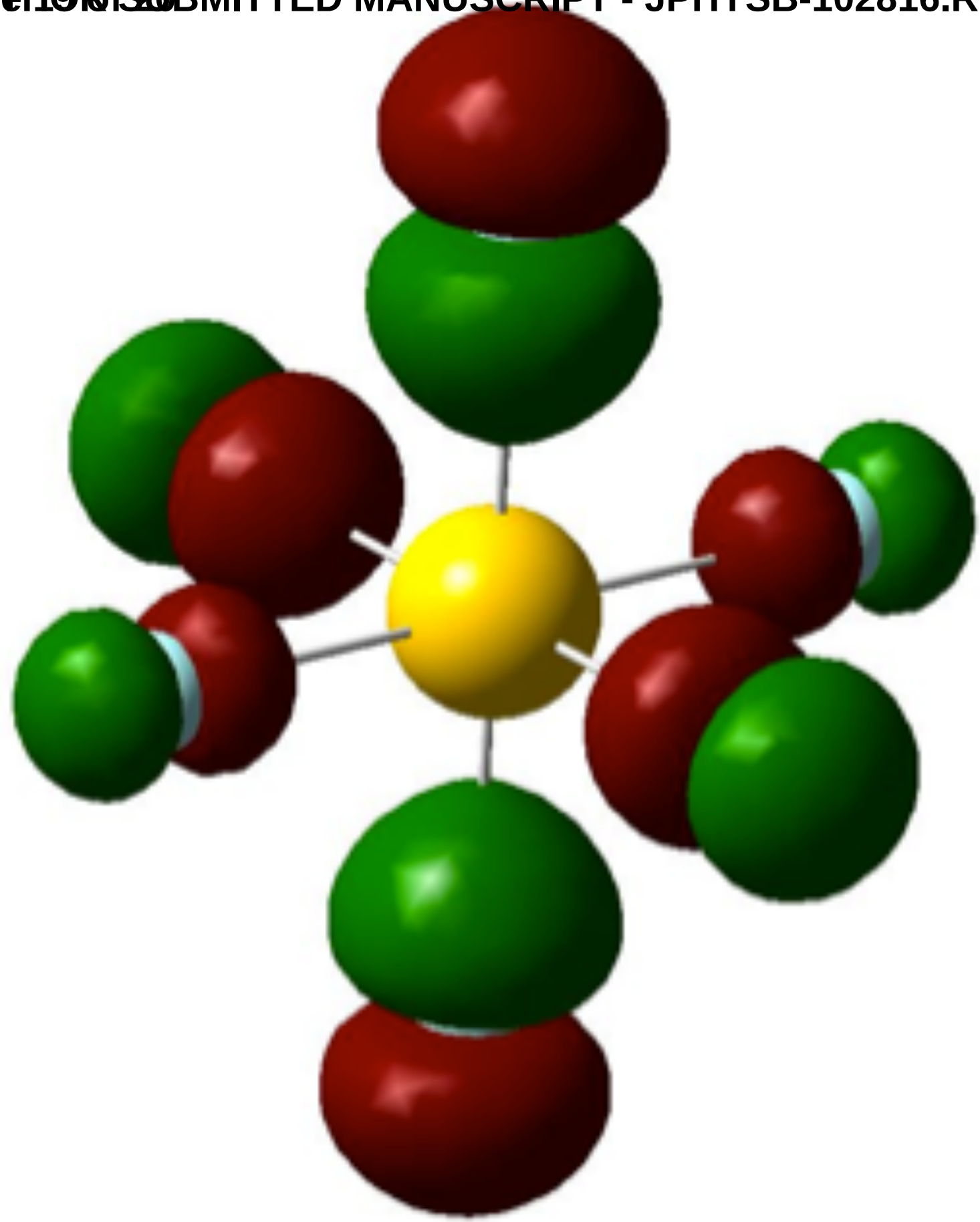

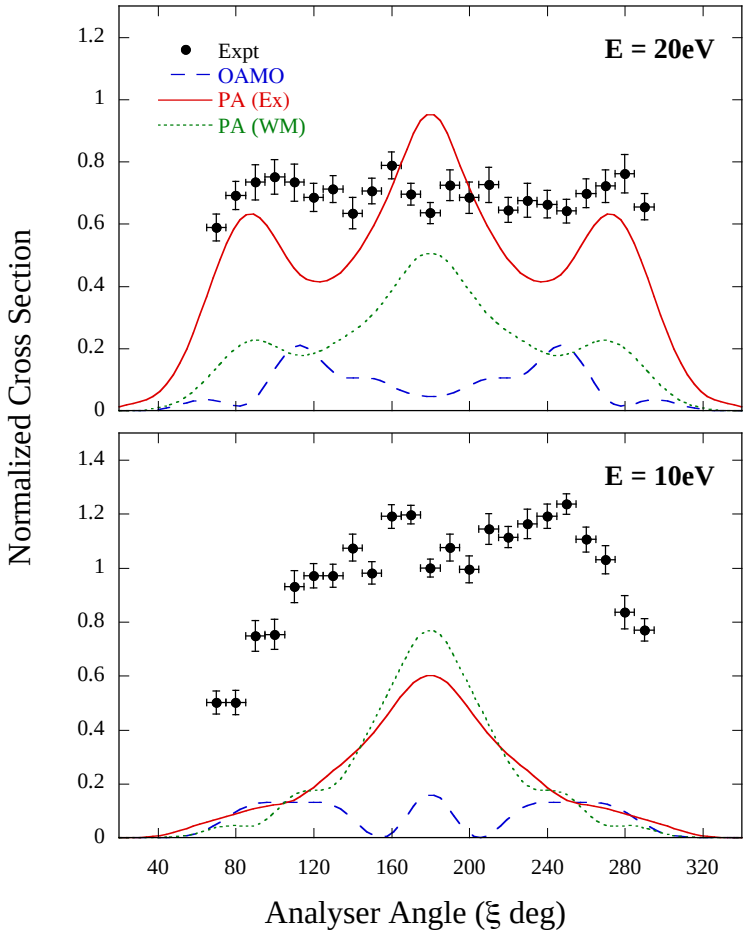
Expt
OAMO
PA (Ex)
PA (WM)
E = 20eV
E = 10eV
Normalized Cross Section
Analyser Angle (ξ deg)
0
0.2
0.4
0.6
0.8
1
1.2
1.4
40
80
120
160
200
240
280
320